Bendable n-Type Metallic Nanocomposites with Large Thermoelectric Power Factor

Yani Chen, Minhong He, Bin Liu, Guillermo C. Bazan, Jun Zhou,* and Ziqi Liang**

Thermoelectric (TE) materials that directly convert heat into electricity and vice versa, have attracted significant interest because of their potential applications in waste heat recovery, solar thermal utilization, as well as alternative power generation and refrigeration technologies.[1–4] There are two key parameters used to characterize the performance of TE materials:[5] one is the dimensionless figure of merit ($ZT = S^2\sigma T/\kappa$), which determines the energy-conversion efficiency, and the second is the power factor ($PF = S^2\sigma$), which is proportional to the maximum output power, where S is the Seebeck coefficient, σ is the electrical conductivity, T is the absolute temperature, and κ is the thermal conductivity including contributions from both phonons and electrons.

Traditional commercial TE materials are inorganic semiconductors, such as Bi_2Te_3, PbTe, and SiGe alloys, for which the ZT and PF are on the order of one and several thousand $\mu W\ m^{-1}\ K^{-2}$, respectively.[6–8] Potential drawbacks of inorganic systems include high cost, scarcity, toxicity, brittleness, and scalability challenges.[9–11] Their organic TE counterparts may be able to circumvent these challenges by offering the possibility of low-cost fabrication from solution and light-weight devices, thus paving the way for producing flexible TE modules by high-throughput methods.[12–15] However, the intrinsically lower electrical conductivity of organic semiconductors provides a challenge for improving the PF and ZT. Organic–inorganic TE nanocomposites (TENCs) have therefore been recently developed to resolve the above issues. This design strategy seeks to combine the high electrical conductivity of the inorganic component with the low thermal conductivity, rational molecular design, and mechanical flexibility afforded by organic materials. Moreover, the coupling between organic and inorganic parts can lead to a simultaneous improvement of the electrical conductivity and the Seebeck coefficient,[16,17] while the internal interfaces introduce phonon-boundary scattering and reduce the lattice thermal conductivity.

Most commonly used organic components for TENCs include π-conjugated polymers, such as poly(3-hexylthiophene) (P3HT), polyaniline (PANI), and poly(3,4-ethylenedioxythiophene):poly(styrenesulfonate) (PEDOT:PSS). For instance, Zhang et al. incorporated both n- and p-type Bi_2Te_3 ball-milled powders into commercial PEDOT:PSS, and obtained PF values of 70 and 40 $\mu W\ m^{-1}\ K^{-2}$, respectively.[18] See et al. prepared water-soluble p-type PEDOT:PSS/Te nanocomposites, which exhibited increased electrical conductivity while retaining the low thermal conductivity of PEDOT:PSS, giving a room temperature ZT of around 0.1.[19] Likewise, a p-type PANI/Te composite was found to achieve a PF of 105 $\mu W\ m^{-1}\ K^{-2}$ at room temperature.[20] Hong et al. prepared a p-type $FeCl_3$-doped P3HT/carbon nanotube (CNT) with a PF of 267 $\mu W\ m^{-1}\ K^{-2}$, in which the CNT bundles formed an interconnected network.[21] Insulating polymers, such as poly(vinylidene fluoride) (PVDF), have also been used. By utilizing a vacuum filtration process, flexible PVDF/$Cu_{1.75}Te$ composites were obtained with $S = 9.6\ \mu V\ K^{-1}$, $\sigma = 2490\ S\ cm^{-1}$, and $PF = 23\ \mu W\ m^{-1}\ K^{-2}$.[22] These examples principally introduce TE inorganic semiconductors and, more importantly, high PFs have been achieved predominantly for p-type systems. n-Type TENCs, a necessary prerequisite for constructing TE modules, lag in performance and their PFs seldom exceed 100 $\mu W\ m^{-1}\ K^{-2}$. Very recently, however, the Koumoto group has reported a PF of 450 $\mu W\ m^{-1}\ K^{-2}$ for the n-type hybrid superlattice $TiS_2/[(hexylammonium)_x(H_2O)_y(DMSO)_z]$, which was fabricated by electrochemical intercalation and solvent-exchange processes.[23] Also, PEDOT/CNTs hybrids have shown high PFs up to 1000 $\mu W\ m^{-1}\ K^{-2}$ after treatment with n-type tetrakis(dimethylamino)ethylene (TDAE) dopant.[24] The Zhu group electrochemically deposited a coordination polymer from ethylenetetrathiolate and Ni, with a $PF = 453\ \mu W\ m^{-1}\ K^{-2}$ owing to improved structural ordering.[25] Metals, which present opportunities of comparatively low cost and high conductivity, are less frequently encountered in TENCs. One exception are p-type PEDOT:PSS/Ag NWs bulk TE hybrids obtained by cryogenic grinding and a spark plasma sintering processes,[26] which reached a PF of 2.85 $\mu W\ m^{-1}\ K^{-2}$, most likely due to the low Ag loading content. This overview of recent highlights points to growing opportunities for diversifying the range of materials incorporated within TENCs and the need to understand how to best achieve n-type TE materials that are compatible with simple scale-up fabrication protocols.

In response to the preceding comments, we report here a simple method of preparing n-type TENCs containing one-dimensional Ni NWs embedded within an insulating PVDF matrix, which do not require doping and can be obtained from

Y. Chen, M. He, Prof. Z. Liang
Department of Materials Science
Fudan University
Shanghai 200433, P. R. China
E-mail: zqliang@fudan.edu.cn
B. Liu, Prof. J. Zhou
Center for Phononics and Thermal Energy Science
School of Physics Science and Engineering
Tongji University
Shanghai 200092, P. R. China
E-mail: zhoujunzhou@tongji.edu.cn
Prof. G. C. Bazan
Department of Chemistry and Biochemistry & Department of Materials Science
University of California at Santa Barbara
CA 93106–9510, USA
E-mail: bazan@chem.ucsb.edu

DOI: 10.1002/adma.201604752

solution to yield highly bendable thin films. TENCs containing 80 wt% Ni NWs yield a notably high σ of 4701 S cm^{-1} and a large S of –20 μV K^{-1}, resulting in a PF of 200 μW m^{-1} K^{-2} at room temperature. This PF value is among the highest observed for n-type TENCs. It is also worth noting that σ and S exhibit an unusual decoupling phenomenon relative to the Ni content, which is interpreted by favorable carrier transport across a percolated network within the nanocomposites.

We chose PVDF as the matrix owing to its superior film-forming property, plasticity, and thermal stability.[27] Five different sets of TENCs were obtained by mixing Ni NWs with PVDF powder in dimethylformamide (DMF) solution, followed by drying in an aluminum mold inside a N_2-filled glovebox. Given the propensity of Ni toward oxidation, the TENCs were immersed in an ethanol solution of hydrazine hydrate prior to use. The Ni content in the composites was varied from 20, 35, 50, 65, to 80 wt%, and the thickness of these TENC films was kept at around 30 μm. Note that when the Ni NWs loading was higher than 80 wt%, the sample became very brittle and easily cracked when peeled off from the substrate, as shown in Figure S1a in the Supporting Information.

A typical photograph of an as-fabricated Ni/PVDF TENC film, shown in **Figure 1**a, reveals that the film is free-standing and has a smooth surface with an area of approximately 4 cm^2. The film is highly bendable and hard to deform, thus demonstrating its relevance for flexible and portable TE modules. To quantify the bendability, Figure S1b,c (Supporting Information) shows photographs of Ni (80 wt%)/PVDF TENC films inside two tubes of different radii, the smallest of which is 4.7 mm.[28] Upon removal from the tube, the film preserves its original shape and smooth surface without any deformation nor cracks owing to the ductility of the metallic Ni NWs (Figure S1d). Field-emission scanning electron microscopy (FE-SEM) was used to examine the morphological details. As shown by the top-view SEM in Figure 1d–f, the Ni NWs are randomly distributed within the PVDF matrix, from which typical three-dimensional (3D) percolation networks could be anticipated that depend on the volume fractions of Ni. As shown in Figure 1b–d, when the Ni content is less than 50 wt%, most Ni NWs are isolated with sporadic connections between them. As the Ni content increases to 65 wt%, more connections are formed, as shown in Figure 1e. At 80 wt%, the Ni NWs are entangled, as indicated in Figure 1f, leading to conditions that favor electrical transport.

The samples were further analyzed by X-ray diffraction (XRD). As shown in **Figure 2**, all five Ni/PVDF TENCs show three strong diffraction peaks at 44.5, 51.8, and 76.4°, corresponding to the (111), (200), and (220) reflections of Ni, respectively (JCPDS no. 04–0850). Moreover, these peaks increase in intensity when the Ni content increases from 20 to 80 wt%. The absence of any diffraction peaks at 37.2, 43.2, 62.8, 75.3, and 79.3° indicates the absence of NiO, which would decrease the electrical conductivity.

The room-temperature average TE properties of the Ni/PVDF TENCs as a function of Ni content are presented in **Figure 3** (see Experimental Section for characterization details and Supporting Information for description of the measurements). As shown in Figure 3a, σ increases from 15 S cm^{-1} to 4701 S cm^{-1} as the Ni content changes from 20 wt% to 80 wt%. Owing to the larger density of Ni (8.90 g cm^{-3}) than that of PVDF (1.78 g cm^{-3}), the volume fraction (p) of Ni NWs in the TENCs is much lower than their corresponding weight percentage. That is, increases in Ni content – from 20, 35, 50, 65 to 80 wt% lead to increased p – from 0.0476, 0.0972, 0.167, 0.271 to 0.445, respectively. The σ values of Ni/PVDF TENCs were fitted to the universal power scaling law of percolation theory:

$$\sigma(T) = \sigma_0(T)(p - p_c)^u \quad (1)$$

where $\sigma_0(T) = 2.98 \times 10^4$ S cm^{-1} at room temperature is the fitted pre-factor and is related to the intrinsic σ of Ni NWs,[29] $p_c = 0.0476$ (corresponding to 20 wt%) is the fitted percolation threshold, which is very close to the simulated value of 0.043 by the 3D Monte Carlo method when the average aspect ratio of Ni NWs is around 15 (Figure 1b–d).[30]

The fitted lines were in excellent agreement with the experimental data for $u = 2$, corresponding to a parabolic dependence of

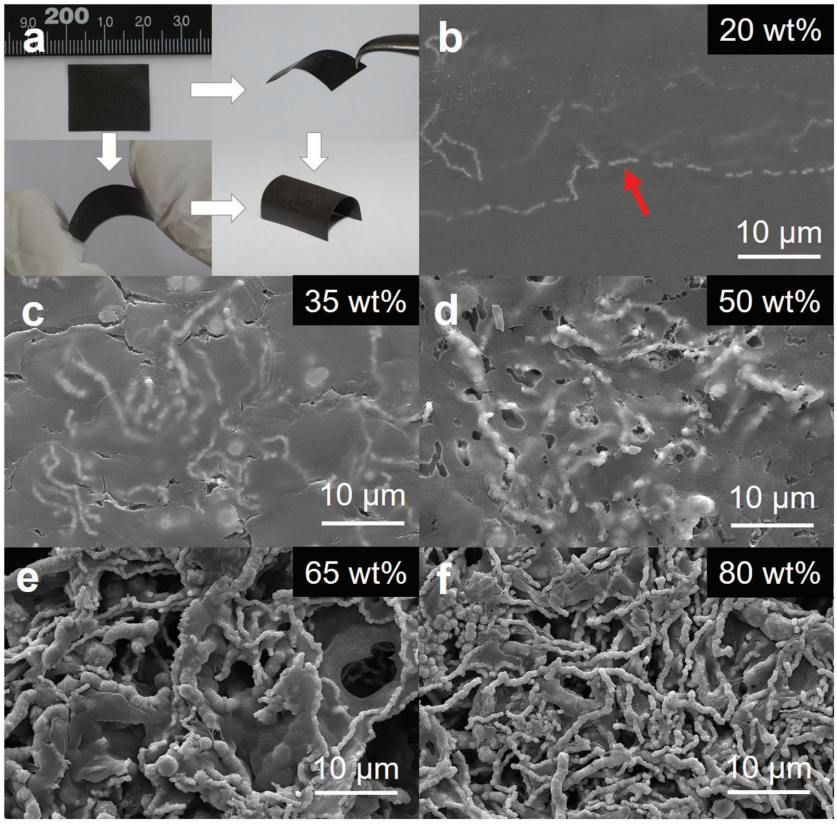

Figure 1. a) Typical photographs of highly bendable Ni/PVDF TENC film. d–f) Top-view SEM images of the Ni/PVDF TENCs with different contents of Ni NWs. Ni NWs are denoted by the red arrow.

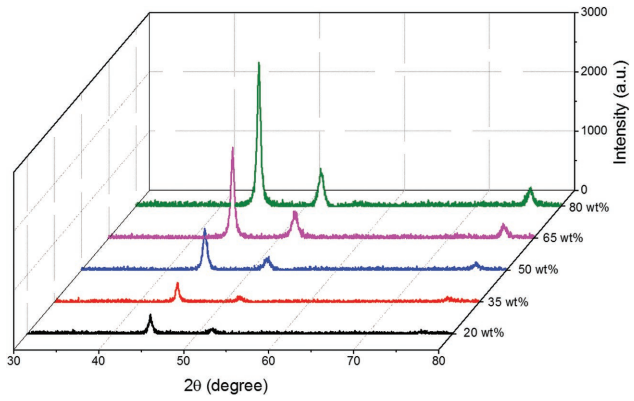

Figure 2. XRD patterns of Ni/PVDF TENCs with different contents of Ni NWs.

$\sigma(T)$, thus providing strong evidence for the formation of a 3D percolation network.[31] All the Ni/PVDF TENCs exhibit negative values of S (Figure 3a), which is given by the slope of the straight fitting line of $\Delta V/\Delta T$. Therefore the majority of charge carriers are electrons. S increases from −7.5 to −20.6 μV K^{-1} with increasing Ni content; interestingly, −20.6 μV K^{-1} approaches the value of neat Ni. Currently, we lack a complete theory that can successfully explain the dependence of S on the Ni volume fraction. According to the heterogeneous model,[32] however, the overall S is a weighted average over those of individual Ni NWs and junctions between neighboring NWs. Once the Ni content reaches the percolation threshold, the S of the Ni NWs becomes dominant. The above simultaneous increase in both σ and S is in accordance with previous reports on CNTs-based nanocomposites.[16,17] Figure 3b exhibits a gradual increase in PF when the Ni content ≤50 wt%, yet there is a parabolic enhancement of PF when the Ni content ≥65 wt%. As a result, the highest PF of 200 μW m^{-1} K^{-2} is obtained at 80 wt% Ni NWs, whereby p is far greater than p_c.

Figure 4 presents how the average TE properties of optimal Ni (80 wt%)/PVDF TENCs change in the temperature range of 300–380 K. The value of σ decreases with increasing temperature, which is typical metallic behavior and originates from enhanced electron–phonon scattering in the Ni NWs (Figure 4a). The experimental data of σ can be modeled with the temperature dependent characteristic of metals:

$$\sigma_0(T) = \sigma_0(293\ \mathrm{K}) / [1 + \alpha(T - 293\ \mathrm{K})] \quad (2)$$

where α = 0.0059 K^{-1} is the temperature coefficient of resistivity.[33] Figure 4b shows that the absolute S of the nanocomposites increases with temperature. The experimental results of S also fit the dependence:

$$S = aT + bT^{3/2} \quad (3)$$

where the first term comes from the electron diffusion, which is proportional to the temperature T, and the second term is induced by electron–magnon collisions, which is called the magnon-drag effect.[34] The fitting parameters a = −0.041 μV K^{-2} and b = −0.0015 μV K$^{-5/2}$ are used. As a result, the PF of Ni/PVDF TENCs shows a positive temperature dependence, reaching a maximum PF of 220 μW m^{-1} K^{-2} at 380 K (Figure 4c).

Owing to the high sensitivity to the sample preparation method and the absence of established simulation models, it has been technically challenging to accurately measure the in-plane κ by conventional techniques. Thus, most works based on organic/hybrid TEs have provided either the out-of-plane κ or the PF value.[18,19,21,22] Given the homogeneous nature of our Ni/PVDF TENCs made from vigorous mixing in solution, we believe the difference between the out-of-plane and in-plane κ values is relatively small. Therefore, we used the out-of-plane κ as an estimate of the in-plane one. **Figure 5** shows the temperature dependence of the calculated out-of-plane κ of the Ni (80 wt%)/PVDF TENCs. The methods and data are shown in the Experimental Section and Supporting Information, respectively. The average κ is 0.55 W m^{-1} K^{-1} at room temperature and it remains nearly constant over the whole temperature range. Furthermore, it is smaller than that of bulk Ni (ca. 90 W m^{-1} K^{-1}).[35] The reasons for these trends may be rationalized as follows: i) nanostructured interfaces are present in the TENCs, which cause significant phonon-boundary scattering; ii) the thermal boundary resistance in these TENCs is large, which strongly hinders thermal transport; and iii) given

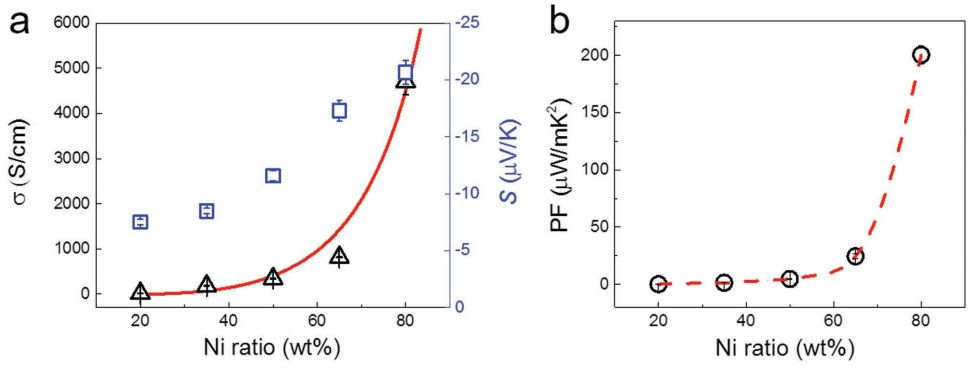

Figure 3. TE performance of Ni/PVDF TENCs as a function of Ni content at room temperature. a,b) The dependence of the average electrical conductivity (triangles) (a), Seebeck coefficient (squares) (a), and power factor (circles) (b) on the Ni NWs content. The points represent the experimental data, and the fitted line in (a) corresponds to the simulated results. Note that the dashed line in (b) is a guide to the eye.

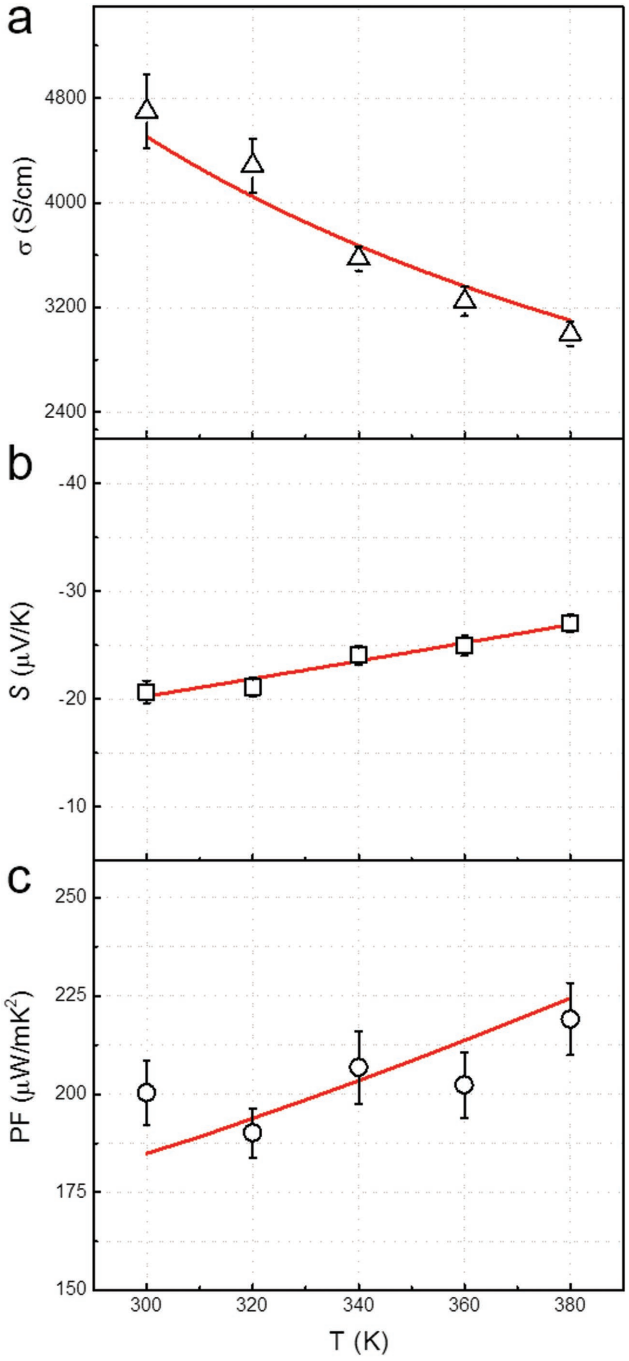

Figure 4. Temperature dependence of average TE properties of the optimal Ni (80 wt%)/PVDF TENCs. a) Electrical conductivity (triangles), b) Seebeck coefficient (squares), and c) power factor (circles). The points are experimental data, and the fitted lines are the corresponding simulated results.

the lower κ of PVDF than that of the Ni NWs, a considerably low κ can thus be obtained in the TENCs, according to the effective medium theory.[36] As a result, remarkably high PFs and a low κ could be simultaneously achieved in these TENCs, yielding the best ZT of around 0.15 at 380 K.

In conclusion, we have successfully fabricated highly flexible yet non-deformable n-type TENCs of Ni NWs/PVDF

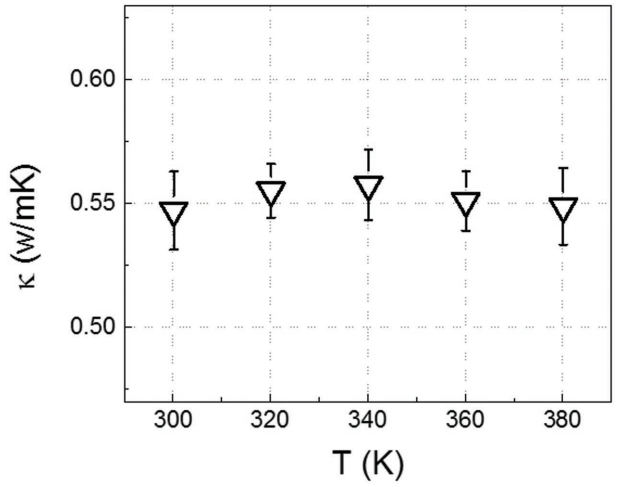

Figure 5. Temperature dependence of out-of-plane thermal conductivity of the optimal Ni (80 wt%)/PVDF TENCs.

without the need for a doping treatment. The electrical conductivity of the nanocomposites increases dramatically from 15 to 4701 S cm^{-1} when the content of the Ni NWs is increased from 20 to 80 wt%. This trend is consistent with the formation of a percolated network of Ni NWs in the films through which carrier transport occurrs. Interestingly, the maximum Seebeck coefficient value obtained is −20.6 μV K^{-1}, which is similar to that of neat Ni. As a result, impressively large power factors of 200 and 220 μW m^{-1} K^{-2} are obtained at room temperature and 380 K, respectively. Given the low thermal conductivity of 0.55 W m^{-1} K^{-1}, a maximum ZT of 0.15 is achieved at 380 K in these TENCs. Both the power factor and ZT values are among the highest achieved for n-type TENCs.[23–25] This work provides the first demonstration that the combination of an insulating polymer and an inorganic metal, each of which is a poor TE material, can be brought together to form a nanocomposite with unexpectedly outstanding TE properties.

Experimental Section

Chemicals and Materials: All the chemicals used in the experiments were purchased and used without further purification, including Ni NWs (JCNANO Tech Co., Ltd), poly(vinylidene fluoride) (PVDF) (M_w = 900 kDa, Arkem, Ltd), dimethylformamide (DMF) (Adamas-beta), and Ni nanowires (Nanjing Jicang Nano Technology Co., Ltd).

Fabrication of Ni/PVDF TENCs: A typical fabrication procedure of Ni/PVDF TENCs is provided: PVDF (0.1 g) was first dissolved into DMF (0.9 g) in a 50 mL flask under vigorous stirring at 70 °C for 3 h. Subsequently, different quantities of Ni NWs at 20, 35, 50, 65, and 80 wt% were dispersed into the PVDF solution under mild mechanical stirring at room temperature over a period of 1 h. Ni/PVDF TENCs were obtained by drop-casting the mixture solution into aluminum molds inside a N_2-filled glovebox, followed by vacuum drying at 40 °C overnight. The resulting TENCs films were subsequently peeled off from the aluminum molds and pressed under 15 MPa for 2 min. Afterwards, these TENCs were transferred into a N_2-filled glovebox, and then immersed in an ethanol solution of hydrazine hydrate (16 vol%) for 5 min. Finally, the samples were thermal annealed at 110 °C for 30 min prior to use.

Characterization and Measurements: The electrical properties of the nanocomposites were measured in the temperature range of 280 to 380 K by using a custom-built apparatus as illustrated in Figure S2

(Supporting Information). A four-probe technique was used to measure the electrical conductivity on a multimeter (Keithley 2010) and a source meter (Keithley 2400). The Seebeck coefficient was measured by heating one resistor block while simultaneously measuring the generated temperature gradient (ΔT) and thermoelectric voltage (ΔV). The thermal diffusivity (D) was acquired on a Netzsch LFA 467 Nanoflash apparatus based on the xenon flash method in the Application Laboratory of Netzsch Scientific Instruments Trading (Shanghai) Ltd. and the certified data are provided in the Supporting Information. The specific heat (C_p) was determined on a TA Q2000 differential scanning calorimeter, whereas the density (ρ) was measured by Archimedes' method. The thermal conductivity was then calculated by using the equation of $\kappa = D \times C_p \times \rho$. Each data point of the electrical and thermal results was measured three times and then averaged for discussion, as shown in Table S1 (Supporting Information). Field-emission scanning electron microscopy images were acquired on a JEOL JSM-6701F at an accelerating voltage of up to 30 kV. X-ray diffraction pattern data for 2θ values were collected with a Bruker AX D8 Advance diffractometer with nickel-filtered Cu Kα radiation ($\lambda = 1.5406$ Å).

Supporting Information

Supporting Information is available from the Wiley Online Library or from the author.

Acknowledgements

Y.C. and M.H.contributed equally to this work. This work is sponsored by the National Natural Science Foundation of China (NSFC) under grant No. 51673044 (Z.L.). J.Z. acknowledges the support from the National Natural Science Foundation of China under grant No.11404244; the program for New Century Excellent Talents in Universities Grant No. NCET-13-0431; and the program for Professor of Special Appointment (Eastern Scholar) at Shanghai Institutions of Higher Learning (Grant No. TP2014012).

Received: September 4, 2016
Revised: September 23, 2016
Published online: November 11, 2016

[1] M. S. Dresselhaus, G. Chen, M. Y. Tang, R. Yang, H. Lee, D. Wang, Z. Ren, J.-P. Fleurial, P. Gogna, *Adv. Mater.* **2007**, *19*, 1043.
[2] G. J. Snyder, E. S. Toberer, *Nat. Mater.* **2008**, *7*, 105.
[3] F. J. DiSalvo, *Science* **1999**, *285*, 703.
[4] L. E. Bell, *Science* **2008**, *321*, 1457.
[5] D. M. Rowe, *Thermoelectrics Handbook: Macro to Nano*, CRC Press, Boca Raton, FL, USA **2005**.
[6] W. Liu, K. C. Lukas, K. McEnaney, S. Lee, Q. Zhang, C. P. Opeil, G. Chen, Z. Ren, *Energy Environ. Sci.* **2013**, *6*, 552.
[7] Y. Pei, A. D. LaLonde, N. A. Heinz, G. J. Snyder, *Adv. Energy Mater.* **2012**, *2*, 670.
[8] E. K. Lee, L. Yin, Y. Lee, J. W. Lee, S. J. Lee, J. Lee, S. N. Cha, D. Whang, G. S. Hwang, K. Hippalgaonkar, A. Majumdar, C. Yu, B. L. Choi, J. M. Kim, K. Kim, *Nano Lett.* **2012**, *12*, 2918.
[9] B. T. McGrail, A. Sehirlioglu, E. Pentzer, *Angew. Chem., Int. Ed.* **2015**, *54*, 1710.
[10] L.-D. Zhao, J. He, C.-I. Wu, T. P. Hogan, X. Zhou, C. Uher, V. P. Dravid, M. G. Kanatzidis, *J. Am. Chem. Soc.* **2012**, *134*, 7902.
[11] H. Yang, L. A. Jauregui, G. Zhang, Y. P. Chen, Y. Wu, *Nano Lett.* **2012**, *12*, 540.
[12] O. Bubnova, X. Crispin, *Energy Environ. Sci.* **2012**, *5*, 9345.
[13] Y. Chen, Y. Zhao, Z. Liang, *Energy Environ. Sci.* **2015**, *8*, 401.
[14] Q. Zhang, Y. Sun, W. Xu, D. Zhu, *Adv. Mater.* **2014**, *26*, 6829.
[15] M. He, F. Qiu, Z. Lin, *Energy Environ. Sci.* **2013**, *6*, 1352.
[16] Q. Yao, Q. Wang, L. Wang, L. Chen, *Energy Environ. Sci.* **2014**, *7*, 3801.
[17] H. Wang, S.-i. Yi, X. Pu, C. Yu, *ACS Appl. Mater. Interfaces* **2015**, *7*, 9589.
[18] B. Zhang, J. Sun, H. E. Katz, F. Fang, R. L. Opila, *ACS Appl. Mater. Interfaces* **2010**, *2*, 3170.
[19] K. C. See, J. P. Feser, C. E. Chen, A. Majumdar, J. J. Urban, R. A. Segalman, *Nano Lett.* **2010**, *10*, 4664.
[20] Y. Wang, S. M. Zhang, Y. Deng, *J. Mater. Chem. A* **2016**, *4*, 3554.
[21] C. T. Hong, W. Lee, Y. H. Kang, Y. Yoo, J. Ryu, S. Y. Cho, K.-S. Jang, *J. Mater. Chem. A* **2015**, *3*, 12314.
[22] C. Zhou, C. Dun, Q. Wang, K. Wang, Z. Shi, D. L. Carroll, G. Liu, G. Qiao, *ACS Appl. Mater. Interfaces* **2015**, *7*, 21015.
[23] C. Wan, X. Gu, F. Dang, T. Itoh, Y. Wang, H. Sasaki, M. Kondo, K. Koga, K. Yabuki, G. J. Snyder, R. Yang, K. Koumoto, *Nat. Mater.* **2015**, *14*, 622.
[24] H. Wang, J.-H. Hsu, S.-I. Yi, S. L. Kim, K. Choi, G. Yang, C. Yu, *Adv. Mater.* **2015**, *27*, 6855.
[25] Y. Sun, L. Qiu, L. Tang, H. Geng, H. Wang, F. Zhang, D. Huang, W. Xu, P. Yue, Y.-S. Guan, F. Jiao, Y. Sun, D. Tang, C.-a. Di, Y. Yi, D. Zhu, *Adv. Mater.* **2016**, *28*, 3351.
[26] Y. Liu, Z. Song, Q. Zhang, Z. Zhou, Y. Tang, L. Wang, J. Zhu, W. Luo, W. Jiang, *RSC Adv.* **2015**, *5*, 45106.
[27] P. Martins, A. C. Lopes, S. Lanceros-Mendez, *Prog. Polym. Sci.* **2014**, *39*, 683.
[28] K. Suemori, S. Hoshino, T. Kamata, *Appl. Phys. Lett.* **2013**, *103*, 153902.
[29] M. Foygel, R. D. Morris, D. Anez, S. French, V. L. Sobolev, *Phys. Rev. B* **2005**, *71*, 104201.
[30] N. Hu, Z. Masuda, C. Yan, G. Yamamoto, H. Fukunaga, T. Hashida, *Nanotechnology* **2008**, *19*, 215701.
[31] T. Nakayama, K. Yakubo, R. L. Orbach, *Rev. Mod. Phys.* **1994**, *66*, 381.
[32] A. B. Kaiser, *Phys. Rev. B* **1989**, *40*, 2806.
[33] H. A. Radi, J. O. Rasmussen, *Principles of Physics: For Scientists and Engineers*, Springer Verlag, Berlin, Germany **2013**.
[34] G. N. Grannemann, L. Berger, *Phys. Rev. B* **1976**, *13*, 2072.
[35] Wikipedia, https://en.wikipedia.org/wiki/Thermal_conductivities_of_the_elements_(data_page).
[36] C.-W. Nan, G. Liu, Y. Lin, M. Li, *Appl. Phys. Lett.* **2004**, *85*, 3549.